EJN
European Journal of Neuroscience

European Journal of Neuroscience, Vol. 27, pp. 3095–3108, 2008 doi:10.1111/j.1460-9568.2008.06297.x

A novel role for MNTB neuron dendrites in regulating action potential amplitude and cell excitability during repetitive firing

Richardson N. Leão,[1,*] Ricardo M. Leão,[2] Luciano F. da Costa,[3] S. Rock Levinson[4] and Bruce Walmsley[1]
[1]Synapse and Hearing Laboratory, The John Curtin School of Medical Research, The Australian National University, Canberra, ACT, Australia 0200
[2]Departamento de Fisiologia, Faculdade de Medicina de Ribeirão Preto, Universidade de São Paulo, Ribeirão Preto, SP, Brazil
[3]Grupo de Instrumentação e Informática, Instituto de Física, Universidade de São Paulo, São Carlos, SP, Brazil
[4]Department of Physiology and Biophysic UCHSC at Fitzsimons, Denver, CO, USA

Keywords: active dendrite, MNTB, repetitive firing, sodium currents, sodium imaging

Abstract

Principal cells of the medial nucleus of the trapezoid body (MNTB) are simple round neurons that receive a large excitatory synapse (the calyx of Held) and many small inhibitory synapses on the soma. Strangely, these neurons also possess one or two short tufted dendrites, whose function is unknown. Here we assess the role of these MNTB cell dendrites using patch-clamp recordings, imaging and immunohistochemistry techniques. Using outside-out patches and immunohistochemistry, we demonstrate the presence of dendritic Na^+ channels. Current-clamp recordings show that tetrodotoxin applied onto dendrites impairs action potential (AP) firing. Using Na^+ imaging, we show that the dendrite may serve to maintain AP amplitudes during high-frequency firing, as Na^+ clearance in dendritic compartments is faster than axonal compartments. Prolonged high-frequency firing can diminish Na^+ gradients in the axon while the dendritic gradient remains closer to resting conditions; therefore, the dendrite can provide additional inward current during prolonged firing. Using electron microscopy, we demonstrate that there are small excitatory synaptic boutons on dendrites. Multi-compartment MNTB cell simulations show that, with an active dendrite, dendritic excitatory postsynaptic currents (EPSCs) elicit delayed APs compared with calyceal EPSCs. Together with high- and low-threshold voltage-gated K^+ currents, we suggest that the function of the MNTB dendrite is to improve high-fidelity firing, and our modelling results indicate that an active dendrite could contribute to a 'dual' firing mode for MNTB cells (an instantaneous response to calyceal inputs and a delayed response to non-calyceal dendritic excitatory postsynaptic potentials).

Introduction

The medial nucleus of the trapezoid body (MNTB) has attracted considerable attention in the field of synaptic physiology due to the giant calyx of Held synaptic connection, which provides the ability to obtain direct recordings from the presynaptic terminal and postsynaptic cell (Forsythe, 1994; von Gersdorff & Borst, 2002). In contrast to the exuberant presynaptic terminal, MNTB principal neurons are simple spherical cells exhibiting one or two short dendrites (Smith *et al.*, 1998). While MNTB neurons receive both excitatory and inhibitory synaptic terminals onto their soma, the presence of significant functional dendritic inputs has been debated (Smith *et al.*, 1998; Hamann *et al.*, 2003; Leao *et al.*, 2004a,b). Hence, particularly in modelling studies, the principal cell has always been considered as a simple sphere and MNTB dendrites have been ignored (Wang *et al.*, 1998; Leao *et al.*, 2006a,b). Perhaps due to their short length and lack of complexity, MNTB dendrites have also not been considered to perform important computational tasks. However, dendrites can make up to 25% of the principal neuron surface area (Leao, unpublished data), adding considerable capacitance to the neuron and potentially impairing firing. In this study, we show that MNTB dendrites display active conductances (voltage-gated Na^+ channels – NaVch), which contribute to the maintenance of action potential (AP) amplitude during high-frequency firing. In addition, dendritic NaVch may provide a 'dual' firing mode of MNTB neurons in response to calyceal ('quasi' instantaneous APs) and non-calyceal (delayed APs) input.

Correspondence: Dr Richardson N. Leão, *present address below.
E-mail: richardson.leao@ki.se

*Nobel Institute for Neurophysiology, Department of Neuroscience, Karolinska Institute, Retzius väg 8, A3:5, SE-171 77 Stockholm, Sweden.

Received 19 March 2008, revised 23 April 2008, accepted 27 April 2008

Materials and methods

Electrophysiology

Wistar rat brain slices containing the superior olivary complex were obtained as described previously (Leao *et al.*, 2006b). In brief, 12–16 (average 14.2 ± 0.6)-day-old postnatal rats were decapitated according to the Australian National University Animal Ethics Committee protocol. The forebrain and cerebellum were removed and placed in ice-cold hypertonic sucrose solution (Leao *et al.*, 2006b). Transverse slices (200 μm) were made of the MNTB using an oscillating tissue slicer. Slices were incubated for 1 h in normal artificial cerebrospinal fluid (ACSF; in mM: NaCl, 130; KCl, 3; $MgCl_2$, 5; $CaCl_2$, 1;

NaH_2PO_4, 1.25; $NaHCO_3$, 26.2; glucose, 10; constantly bubbled with 95% O_2 and 5% CO_2) at 35°C and subsequently held at room temperature (22–25°C) for electrophysiological recording using glass pipettes filled with a CsCl-based internal solution (in mM: CsCl, 120; NaCl, 4; $MgCl_2$, 4; $CaCl_2$, 0.001; HEPES, 10; Mg-ATP, 3; GTP-Tris, 0.3; EGTA, 10) or K-gluconate-based internal solution (in mM: KCl, 17.5; K-gluconate, 122.5; NaCl, 9; $MgCl_2$, 1; Mg-ATP, 3; GTP-Tris, 0.3; HEPES, 1; EGTA, 0.2); pH was adjusted to 7.2 using CsOH (or KOH for K-gluconate). Data were digitized using Axograph X (Axograph, Sydney, NSW, Australia) and analysed using Matlab (Mathworks, Natick, MA, USA). In order to confirm whether postsynaptic soma and dendrite membranes contain NaVch we pulled outside-out patches from soma and dendritic regions. Only patches that had an input resistance > 400 MΩ were used. We assessed fast-inactivating Na^+ currents in outside-out patches using a 100-mV, 500-ms pre-test voltage step followed by 30-ms voltage steps ranging from −90 to 50 mV in 10-mV increments. Transient Na^+ currents were measured from the peak inward current to the current recorded at the end of the 30-ms voltage steps. Alexa-488 was added to the internal solution to permit the visualization of the dendrite. After establishing the whole-cell mode of recording (by patch-clamping the soma region of principal cells), holding current was applied to set the membrane potential at −60 mV, and we allowed about 15–20 min for the Alexa-488 to diffuse into the dendrite. Patch-pipettes were then quickly retracted to form outside-out patches of the soma region. We then perfused the slice with 3 mM tetraethyl ammonium (TEA) and 50 μM $CdCl_2$ to minimize K^+ and Ca^{2+} currents, and applied the recording protocol described previously. We then applied the same method used to obtain outside-out patches of the soma to extract outside-out patches of dendrites. To ensure that patches were excised from the dendrite and not from neighbouring cell somas, we carefully examined from the fluorescent 'blob' formed by the excision procedure. To assess the role of dendritic NaVch in the firing properties of MNTB neurons we performed current-clamp recordings in which 0.5 μM tetrodotoxin (TTX; Alomone, Israel) was puffed (2 × 10-ms pulses prior to each protocol) onto dendrites and/or soma of principal cells. Current-clamp recordings were obtained using a K-gluconate-based internal solution in whole-cell configuration. Dendrites were identified as previously described, and pipettes used for pressure-injection were placed at least 60 μm away from the soma and only 1 pulse/min (maximum) was applied. Also, in order to minimize the effect of TTX on somatic or axonal channels we placed the injection pipette in parallel with the outlet tubing of the stage bath. Moreover, only cells where the trajectory of identifiable axons was in the opposite direction to the dendrites were used. In some experiments, we applied a current pulse (0.5 nA, 1 ms) using the patch pipette and an electrical stimulus through a bipolar electrode placed on the ipsilateral lateral superior olive in order to elicit antidromic spikes (in the presence of 1 μM CNQX and 50 μM D-AP5). In other experiments, we performed current-clamp recordings during puffing of normal Na^+ ACSF (in a low-Na^+ bath) for cells in which the dendrite and axon ran in opposite directions. We pressure-ejected normal ACSF (enriched with HEPES) onto dendrites opposed to axons while bathing the cells with low Na^+ ACSF (the NaCl was substituted by equimolar choline chloride). All experiments were performed at room temperature.

Na^+ and Ca^{2+} imaging

Changes in intracellular Na^+ concentration were measured using a confocal microscope (LSM 510; Zeiss, Oberkochen, Germany). MNTB neurons were loaded using patch pipettes containing a KCl-based solution (see previous section) supplemented by 0.5 mM of the sodium dye CoroNa Green, and Alexa 555 (Invitrogen, Carlsbad, CA, USA). Confocal imaging was combined with current-clamp recordings of postsynaptic APs during 100 Hz/50 s (onset equal to t = 7 s) calyceal stimulation (using a bipolar electrode placed at the ventral midline of the slice; Leao *et al.*, 2004a,b). CoroNa emission was calibrated in permeablized cells at different Na^+ concentrations using the method described by Meier *et al.* (2006). We also used 5 mM of the Ca^{2+} indicator Oregon Green BAPTA 2 cell impermeant (Invitrogen) in patch pipettes to investigate the presence of excitatory receptors on MNTB neuron dendrites. For these experiments, we pressure-injected 1 mM glutamate at distal dendritic sites (65 ± 11 mm, n = 4) while holding the cell (whole-cell patch-clamp) at −60 mV. In voltage-clamp, if glutamate activated dendritic receptors (synaptic or extrasynaptic), Ca^{2+} would enter the cell through glutamate receptors but not through voltage-gated Ca^{2+} channels and the indicator signal would be restricted (or greater) to distal dendritic regions (implying the presence of dendritic receptors). CoroNa and Oregon Green BAPTA 2 were excited using the 488 line of an argon laser, and the emission was detected through a dichroic mirror (545 nm) and a bandpass filter (500–530 nm). Alexa 555 was used to detect cellular structures without bleaching the Na^+ dye. Images were analysed using ImageJ (NIH) or Matlab (Mathworks). Data are presented as the percentage change in fluorescence divided by the baseline fluorescence ($\Delta F/F_0$) after background subtraction.

Electron microscopy

We investigated the presence of excitatory synaptic contacts on proximal MNTB neurons using electron microscopy. In these experiments, MNTB slices were obtained as described above and from hypertonic sucrose and fixed in 2% glutaraldehyde in 0.1 M sodium cacodylate buffer, pH 7.4 overnight at 4°C and postfixed using 1% osmium tetroxide in 0.1 M sodium cacodylate buffer at room temperature for 90 min. Slices were dehydrated in serial concentrations of acetone, embedded in resin and post-stained in 2% uranyl acetate for 10 min and lead citrate for 8 min. Ultrathin sections containing the MNTB were photographed at magnifications varying from 1 to 50 K.

Immunohistochemistry and histology

Pan-NaV and Na^+/K^+-ATPase immunohistochemistry was used to assess the subcellular localization of the Na^+/K^+-'pump' in MNTB neurons. Slices were obtained as described above from hypertonic sucrose solution, and fixed for 3 h in 4% paraformaldehyde and phosphate-buffered saline (PBS; 17.52 g NaCl, 0.4 g KCl, 100 mL 0.2 M phosphate buffer, 1.9 L distilled water). Slices were blocked using normal donkey serum (1 : 10 PBS-T) for 30 min. Primary antibodies for Pan-specific rabbit polyclonal antibodies (Pan; 1 : 50 PBS-T) were generated against a conserved sequence present in all vertebrate Nav1 isoforms (Dugandzija-Novakovic *et al.*, 1995). We also used primary antibodies against Na^+/K^+ ATPase (raised in rabbit; 1 : 500 PBS-T – Upstate), microtubule-associated protein 2A and B (MAP 2A and B; raised in mice; 1 : 500; Chemicon, Billerica, MA, USA) and vesicular glutamate transporter (V-Glut 1; raised in guinea pig; 1 : 1000; Chemicon). These antibodies were applied to the slices and left overnight in constant agitation at room temperature. Sections were then washed in PBS for 20 min. Fluorescent secondary antibodies (1 : 1000; Invitrogen) were applied to the sections for 1 h in agitation, washed in PBS and sections mounted on glass slides

with 'Vectashield' (Vector, Burlingame, CA, USA). As a negative control, we incubated the sections in secondary antibodies with no previous application of primary antibodies. Using a 'fast' Golgi staining (Golgi-Cox) kit (FD NeuroTechnologies, Ellicott City, MD, USA), we also investigated the morphology and position of MNTB dendrites (Shu *et al.*, 2007).

Compartmental MNTB model

Due to the impossibility of isolating dendritic Na^+ currents in intact cells, we implemented a multicompartment model of the MNTB principal cell based in our anatomical data to investigate the importance of dendritic currents using the *Neuron* Simulation Environment (Hines & Carnevale, 2001). MNTB neurons were modelled with no dendrites and with one primary dendritic cylinder, compartment length (L) equal to 40 μm and diameter ($\varnothing$) equal to 3 μm emerging from the spherical soma ($\varnothing$ = 20 μm). Two thin secondary dendrites (L = 10 μm, $\varnothing$ = 1 μm each) emanated from the distal extremity of the primary dendrite. We also included a cylindrical axonal compartment originating at the soma (L = 20 μm, $\varnothing$ = 2 μm). Each dendritic (and axonal) cylinder was divided into 10 isopotential compartments connected by axial resistances (150 Ω/cm). All compartments had an unspecific leak conductance (0.265 mS/cm^2, reversal potential equal to −70 mV); I_h was implemented on the proximal 20 μm of the primary dendrite (0.37 mS/cm^2, reversal potential equal to −45 mV), soma (0.57 mS/cm^2). Low-threshold K^+ channels were placed at the axon (0.01592 mS/cm^2) and high-threshold K^+ channels at the soma (0.00918 mS/cm^2). NaVch were placed on axons and in some simulations on dendrites but not on the soma (conductance values are shown in Results). We also added NaVch capable of producing persistent and resurgent NaVch using the dynamics shown in Raman & Bean (2001) as MNTB neurons are known to produce these two types of voltage-dependent Na^+ currents (conductance equal to 0.05 mS/cm^2; Leao *et al.*, 2006b). Details on the parameters and active conductances equations of our model can be found in Leao *et al.* (2006a,b).

Na^+ diffusion simulations

We investigated the dynamic changes of external Na^+ concentration on MNTB neurons and the effect of the calyx of Held on Na^+ gradients across the postsynaptic soma. External [Na^+] was arbitrary and equal to 1, and internal [Na^+] was 0 during initial conditions. We used finite difference simulations incorporating: (i) the pre-synaptic calyx; (ii) the postsynaptic MNTB cell (soma and a dendrite); and (iii) the intra- and extracellular media. A total of 60% of the MNTB soma was assumed to be covered by the presynaptic terminal, and the distance between the presynaptic terminal and the postsynaptic cell was constant and equal to 0.2% of the soma diameter (Satzler *et al.*, 2002); dendrite length and diameter were equal to 200% and 10% of the soma diameter, respectively. Simulations were computed using the Scilab mathematical environment (http://www.scilab.org) considering the time–space diffusion equation and using arbitrary time (t) steps:

$$\frac{\delta C(x,y,z,t)}{\delta t} = D(x,y,z)\left(\frac{\delta^2 C(x,y,z,t)}{\delta x^2} + \frac{\delta^2 C(x,y,z,t)}{\delta y^2} + \frac{\delta^2 C(x,y,z,t)}{\delta z^2}\right)$$

A three-dimension orthogonal grid (x, y, z) was used to represent neuronal structures and extra- and intra-cellular regions. Na^+ concentrations are represented by $C(x, y, z)$. The diffusion constant $D(x, y, z)$ was assumed to be 0.5 and 1 for intra- and extracellular media, respectively (Goodman *et al.*, 2005). At t = 0, $[Na^+]_I$ was equal to 0 and $[Na^+]_E$ was equal to 1. Two situations were considered in order to investigate the effect of additional Na^+ supplied by the extracellular medium through the MNTB dendrite: (i) Na^+ channels incorporated only on the MNTB cell soma; and (ii) channels also added to the dendrite. Na^+ was allowed to diffuse through the extra- and intracellular media.

Results

Dendritic outside-out patches contain Na^+ channels

In order to obtain outside-out patches we first patch-clamped the cell soma, waited 20–30 min for dye diffusion and then withdrew the electrode to form a somatic outside-out patch. In contrast to neurons from other brain regions (e.g. hippocampus), MNTB principal cell dendrites are difficult to visualize, and their position and direction are highly variable (Smith *et al.*, 1998; Meier *et al.*, 2006; Fig. 1A). Also, it is impossible to differentiate them from the pre- or postsynaptic axons unless principal cells are filled with appropriate dyes (Leao *et al.*, 2005). Dendrites had an average diameter of 2.6 ± 0.6 μm (n = 24) and could be visualized in some cases up to 80 μm from the cell soma (mean 47.5 ± 5 μm; n = 24; Fig. 1A). Dendrites could run either in the dorsal/ventral or caudal/rostral planes (Fig. 1A). After recording soma patch responses to voltage-steps, we then localized the filled dendrite and used the same method to obtain outside-out patches from MNTB dendrites. MNTB cell membranes do not tolerate these manipulations well (Leao *et al.*, 2005, 2006b); out of 32 cells we were able to obtain 32 soma patches and eight dendritic patches (mean distance from soma equal to 33 ± 2 μm). In agreement to a previous work, Na^+ currents were not observed in any outside-out patch excised from the soma (n = 32; Leao *et al.*, 2005). However, dendritic patches displayed variable, but significant Na^+ currents −108.7 ± 29.9 pA (at −20 mV; n = 8; Fig. 1B). Na^+ currents in dendrite patches generally displayed slow decay and abnormal I–V relationships (data not shown), and we therefore only used these currents as an indicator of the presence/absence of Na^+ currents (Leao *et al.*, 2005, 2006b). In two dendritic patches we were able to apply 1 μM TTX to confirm that the inward current observed in dendrite patches was carried by TTX-sensitive Na^+ channels (Fig. 1C). The I–V curve for the TTX-sensitive current (digital subtraction of currents recorded before and after TTX application) is shown in Fig. 1D. We have also obtained dendritic patches from two P28 rats showing the presence of transient Na^+ current and no observable transient current in the cell somas (see Supplementary material, Fig. S1, A and B). In these animals, at −20 mV, transient currents were equal to −102.35 pA and −79.41 pA (supplementary Fig. S1, A).

Dendritic Na^+ currents maintain AP amplitude during repetitive firing

To study the contribution of dendritic NaVch to the firing properties of MNTB neurons we pressure-ejected TTX, placing the pipette in the vicinity of dendritic branches (see Materials and methods). In order to avoid the blockage of axonal NaVch, we only used cells that we could visualize both dendrite and axon, and verified that these two structures originated and projected in opposite directions. In 60 cells patched for these experiments, only 10 cells displayed distinct axons and dendrites travelling in opposite directions (Fig. 2A). In four cells, we elicited

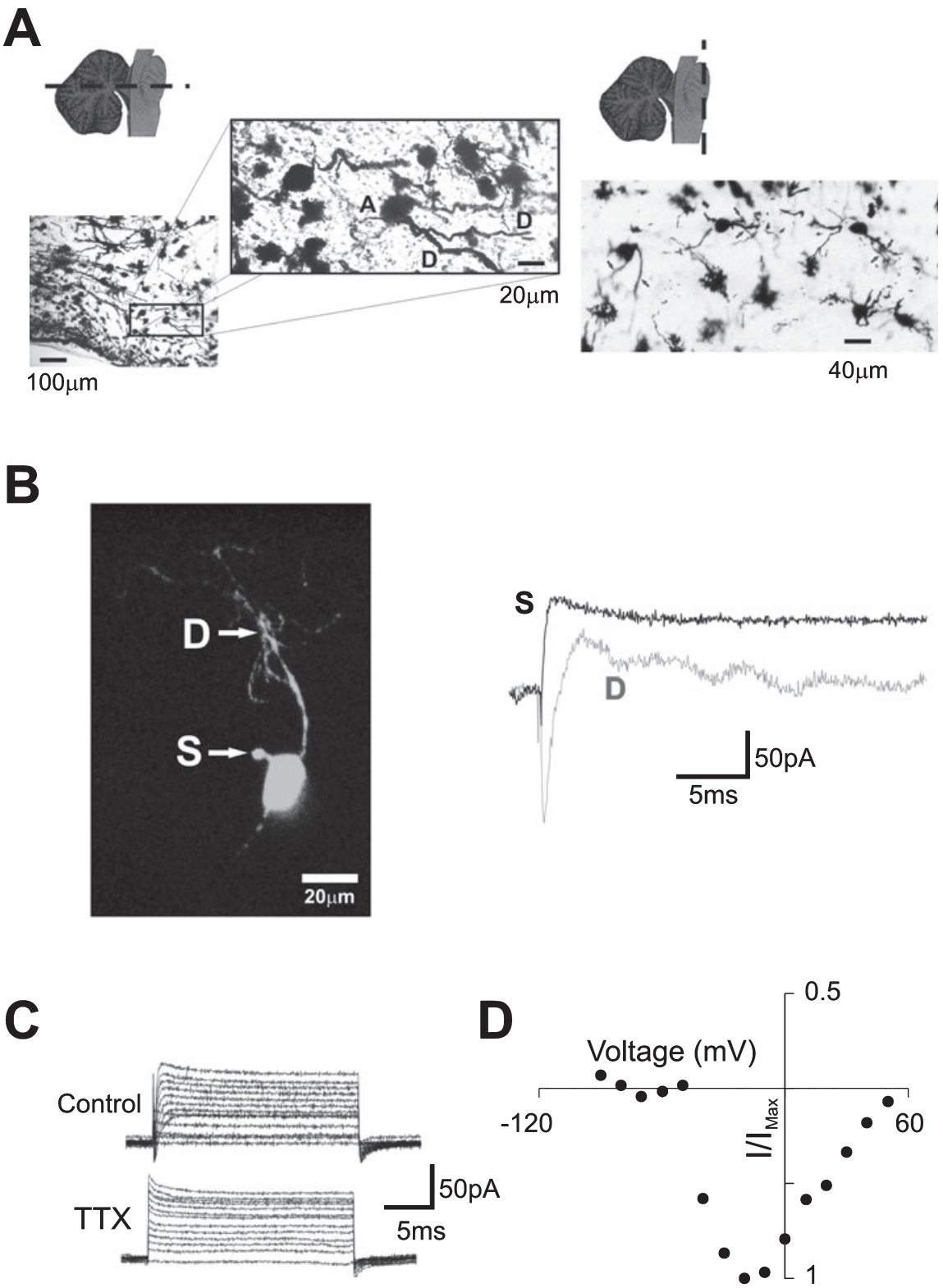

FIG. 1. Na^+ channels are present on dendritic but not somatic MNTB neuron membranes. (A) Photomicrograph of MNTB neurons stained by the Golgi method. Left panels showing a transverse section (A, axon; D, dendrite), while the right panel shows a coronal section (arrows indicate dendrites). (B) Example of somatic (S) and dendritic (D) currents recorded from outside-out patches. The approximate sites of patch extraction for these particular traces are shown left. (C) Example of a dendritic excised patch response to tetrodotoxin (TTX) application. (D) TTX-sensitive current/voltage relationship for the cell shown in (C) (see text for details).

antidromic APs following a current pulse applied to the soma (through the patch pipette). AP amplitudes were substantially decreased in current pulse-elicited spikes after TTX application, with little effect on antidromic spikes: current pulse-elicited spike amplitudes were equal to 71 ± 3 mV in control conditions and 59 ± 4 mV after TTX ejection ($P < 0.03$, paired *t*-test); antidromic spike amplitudes of 47 ± 5 mV in

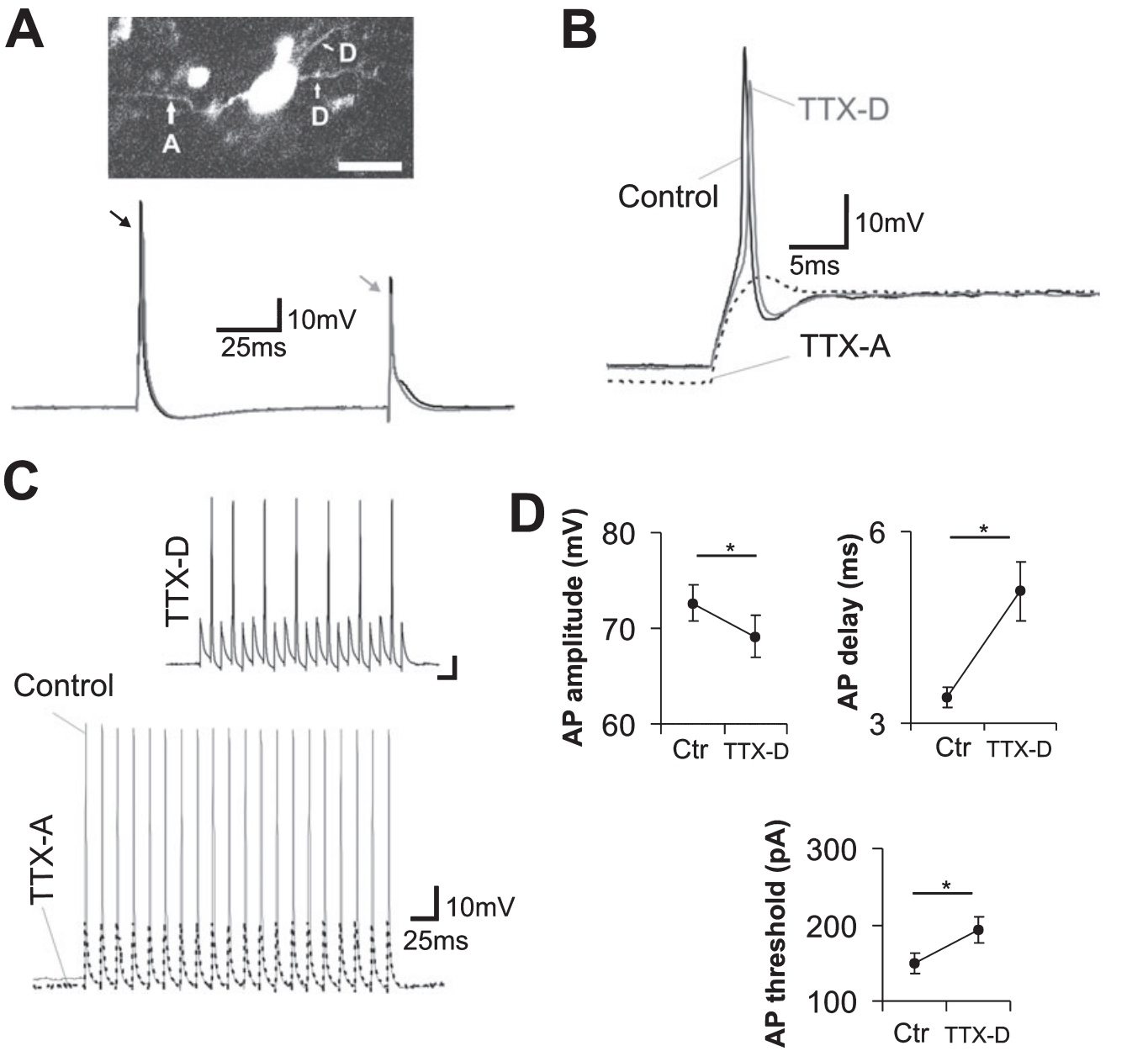

FIG. 2. Blocking of dendritic Na^+ channels impairs action potential (AP) firing. (A) Top panel: Example of an acceptable neuropil configuration for tetrodotoxin (TTX) pressure-injection experiments (axon and dendrite in opposite directions). Bottom panel: Example of a trace showing a delayed AP (elicited by a somatic current injection) after TTX ejected on dendrite (black trace, control; grey trace, TTX). The black arrow indicated the AP generated by current injection and the grey arrow shows the AP elicited by axonal stimulation (antidromic spike). (B) Examples of AP response to 300-pA current steps in control conditions (black solid trace), with TTX ejected onto a dendrite (TTX-D, inset) (bottom left arrow in A) and onto axon (TTX-A, black dashed trace) (top arrow in A). (C) Cell voltage response to 200-Hz/1-nA/0.5-ms current pulses (same conditions as B). Scale bars represent the same value on main panel and inset. (D) Summaries of AP amplitude, delay and threshold (current step amplitude required for firing) in control conditions and after TTX injection near dendrites (* denotes statistical significance, $P < 0.05$, paired *t*-test).

control conditions and 45 ± 3 mV after TTX ejection ($P = 0.04$; Fig. 2A). AP peak time was only altered in spikes generated by the current pulse, suggesting that axonal Na^+ channels were not significantly affected by the TTX ejection around dendrites (delayed by 1.3 ± 0.6 ms after TTX application onto the dendrites; $P < 0.04$, $n = 4$, paired *t*-test; Fig. 2A). AP amplitude (measured from 5% of the peak to the peak amplitude) decreased significantly (during 300-pA steps, from 72.6 ± 1.9 to 69.1 ± 2.2 mV, $P < 0.01$, paired *t*-test) and firing threshold also increased when TTX was distally applied onto dendrites (from 150 ± 13.4 to 193.75 ± 17.5 pA, $P < 0.01$, paired *t*-test; Fig. 2B and D). AP peak times also changed after TTX application (from 3.4 ± 0.2 to 5.1 ± 0.5 ms). No differences were observed in AP half-width (data not shown). During repetitive firing, AP amplitude accommodation (quantified by dividing the amplitude of the first AP by the last AP during a 200-Hz train) did not differ significantly after focal application of TTX (from 1.11 ± 0.02 to 1.15 ± 0.04, 200-Hz pulses). We always observed AP failures after focal TTX injection, but no failures in control conditions (Fig. 2C). TTX injection near the proximal axon abolished APs (Fig. 2B and C). Application of TTX to axons had to be performed about 10–20 μm

from the soma as the unmyelinated portion of MNTB axons does not extend beyond ~10 μm.

Intracellular Na^+ is cleared more rapidly in dendrites than in axons

Intracellular Na^+ concentrations in different neuronal compartments were assessed by loading neurons with the Na^+-sensitive dye CoroNa with subsequent calyceal stimulation. Na^+ concentration during prolonged stimulation was elevated in all compartments (after 33 s of stimulation, t = 40 s); dendrite, $\Delta F/F_0$ = 15 ± 2.6%; soma, $\Delta F/F_0$ = 9.2 ± 3.7%; axon, $\Delta F/F_0$ = 31.6 ± 0.8%; n = 4; Fig. 3A and B). The sharper elevation in Na^+ in the soma and dendrite might be caused by the entry of this ion through AMPA receptors (as the receptor types at this age are mostly permeable to Na^+; Youssoufian *et al.*, 2005). However, intracellular Na^+ (t = 80 s) was rapidly cleared from dendritic and somatic compartments ($\Delta F/F_0$ equal to 7.28% and 3.6%, respectively) but not from axons (16.2 ± 2.3%; $P < 0.01$ when compared with both dendrites and somas; Fig. 3A and B). In one experiment, the cell membrane was permeabilized by extracellular application of gramicidin (in addition to ouabain to block Na^+/K^+ ATPase; see Meier *et al.*, 2006). This technique allows the calibration of the fluorescence emission using known Na^+ concentrations. CoroNa emission can vary significantly in different cells and compartments (Meier *et al.*, 2006). Therefore, we obtained $\Delta F/F_0$ vs. $[Na^+]_I$ in the dendrite, soma and axon. Fluorescence responses of cells loaded with CoroNa were (approximately) linear at different Na^+ concentrations (Fig. 3C), in agreement with results described by Meier *et al.* (2006). Fitting linear functions to $\Delta F/F_0$ vs. $[Na^+]_I$ relationships yielded angular coefficients of 0.0086, 0.0049 and 0.0084 (for dendrite, soma and axon, respectively). Extrapolating the average fluorescence of dendrites, somas and axons using the angular coefficients previously described, $[Na^+]_I$ rises to 17.5 ± 3 mM in dendrites, 18.7 ± 7.5 mM in somas and 37.6 ± 0.9 mM in axons during the stimulation (t = 40 s). Twenty-three seconds after the stimulation (t = 80 s), $[Na^+]_I$ remains high in axons (19.2 ± 2.7 mM), but not in dendrites or somas (8.4 ± 1.7 and 7.3 ± 3 mM, respectively). We simulated the effect of different Na^+ reversal potentials between MNTB axons and dendrites by bathing slices in low-Na^+ ACSF and pressure-ejecting normal Na^+ ACSF in the vicinity of the dendrite (52 ± 2.1 μm from the cell soma). For these experiments, we only used cells where the axon and dendrite ran in opposite directions. After switching the slice bath to low-Na^+ ACSF, we applied 200-Hz current pulses (2.5 ms and 0.5 nA) and pressure-ejected one pulse of normal ACSF 150 ms (t = 250 ms) and 400 ms (t = 500 ms) after the current stimulation onset. We then counted the number of APs in a 50-ms window immediately after the normal ACSF puffs. The first puff of normal ACSF increased the number of APs from 1.33 ± 0.56 to 2.83 ± 0.65 (n = 6, P = 0.02, paired t-test; Fig. 3D and E). In normal ACSF, cells fired 3.5 ± 0.67 APs during the 50 ms after t = 250 ms (this number was significantly greater than the number of APs fired in low-Na^+ ACSF and low-Na^+ ACSF + normal ACSF puff; Fig. 3D). We did not observe changes in resting membrane potential after the ejection of normal ACSF without parallel current stimulation (suggesting that the extra APs were not caused by a mechanical effect of the pressure-ejection).

MNTB dendrites exhibit glutamate receptors

Using a Ca^{2+}-sensitive dye, we then investigated the presence of glutamate receptors on dendrites. In voltage-clamp, $\Delta F/F_0$ for MNTB dendrites (n = 4) was equal to 45.2 ± 8.2% distally (40 ± 3 μm from the dendrite origin) and 6.9 ± 1.6% proximally (P = 0.01; Fig. 4A and B). The presence of dendritic excitatory synaptic terminals was further assessed by electron microscopy. Based on round vesicles in the presynaptic terminal as an indicator of excitatory synapses (Vater, 1995), we observed excitatory synaptic contacts on proximal dendrites (Fig. 4D) in the majority of cells (61% total of 46 cells observed on single electron microscope sections from two animals). An active zone was observed in 75% of those synaptic contacts. In one section, we were able to visualize a dendritic excitatory terminal 20 μm distal to the soma (Fig. 4C). Immunostaining against MAP 2A and B and V-Glut 1 showed the presence of glutamatergic presynaptic vesicles surrounding postsynaptic dendrites (Fig. 4E).

MNTB dendrites are positively labelled by Pan-NaV antibodies while somas show Na^+/K^+ ATPase staining

We applied Pan-NaV antibodies to further confirm the existence of NaVch on dendritic membranes. Anti-Pan-NaV antibodies together with antibodies against MAP 2A and B indicated the presence of NaVch on dendritic membranes (Fig. 5A). We observed tubular and 'ring-like' structures labelled by the Pan-NaV (dendritic NaVch) antibodies associated and non-associated with anti-MAP 2A and B staining (axonal NaVch). The membrane localization of NaVch is implied by the presence of ring-like structures surrounding MAP 2A and B stained neurites (Fig. 5A). Somatic NaVch staining was mostly observed in the cytoplasm, suggesting that channels are assembled at the soma to populate other intracellular domains (axon and dendrite). In general the structures that were not co-localized with anti-MAP 2A and B had diameters smaller than 2 μm (probably marking the postsynaptic axon) or greater than 2 μm (presynaptic axon; Leao *et al.*, 2005). Application of the secondary antibody alone did not yield positive staining when compared with the background (data not shown).

Subsequently, we investigated the possible causes of faster dendritic $[Na]_I$ clearance when compared with axonal $[Na]_I$ clearance. We used

FIG. 3. Na^+ clearance after prolonged firing is faster in dendrites. (A) Panel 1 shows an example of a cell loaded with the Na^+ indicator CoroNa before (t = 5 s), during (t = 40 s) and after (t = 80 s) a train of action potentials (APs). Black lines indicate the scanning region on the soma (S), axon (A) and dendrite (D). Fluorescence ($\Delta F/F_0$) values for the dendrite (D, blue trace), axon (A, red trace) and soma (S, green trace) are shown on Panel 2 (vertical dashed lines indicate the time marks for t equal to 5, 40 and 80 s, horizontal vertical line indicates the resting fluorescence). Panel 3 shows the simultaneous current-clamp recording of the APs evoked by calyceal stimulation for the cell in (A1) and (A2) (inset, voltage-clamp recording at −100 mV of a calyceal EPSP from this cell). (B) Average fluorescence of axonal (red), dendritic (blue) and somatic (green) scans (§ indicates statistical fluorescence differences, $P < 0.05$ between different scan regions on the same category; * shows statistical differences between the same scanning region at different times). (C) Calibration curves ($\Delta F/F_0$ vs. $[Na]_I$) for different scanning regions (same colour coding as B); see text for details. (D) In low-Na^+ ACSF, the pressure application of normal Na^+ ACSF on dendrites improves firing. The black trace is an example of a response to the application of 200-Hz current pulses in low-Na^+ ACSF, while the red trace shows the same cell in low-Na^+ ACSF with the pressure application of normal ACSF at t = 250 ms and 500 ms (the ejection times are indicated by the green dashed line). Inset: same MNTB cell response in normal ACSF (scale bars represent the same values as the large panel). (E) Summary of AP count during a 50-ms window following the first application of normal ACSF to the dendrite (* indicates P = 0.02, paired t-test).

Na^+/K^+ ATPase (alpha 3 subunit; the most abundant type found in brainstem nuclei; Hieber *et al.*, 1991), antibodies anti-MAP 2A and B, and pre-synaptic (anti-V-Glut 1) proteins (Fig. 5B). Na^+/K^+-ATPase staining was mostly restricted to soma membranes, presynaptic terminals and, to a lesser extent, presynaptic axons. Postsynaptic neuropil did not appear to be labelled (Fig. 5B).

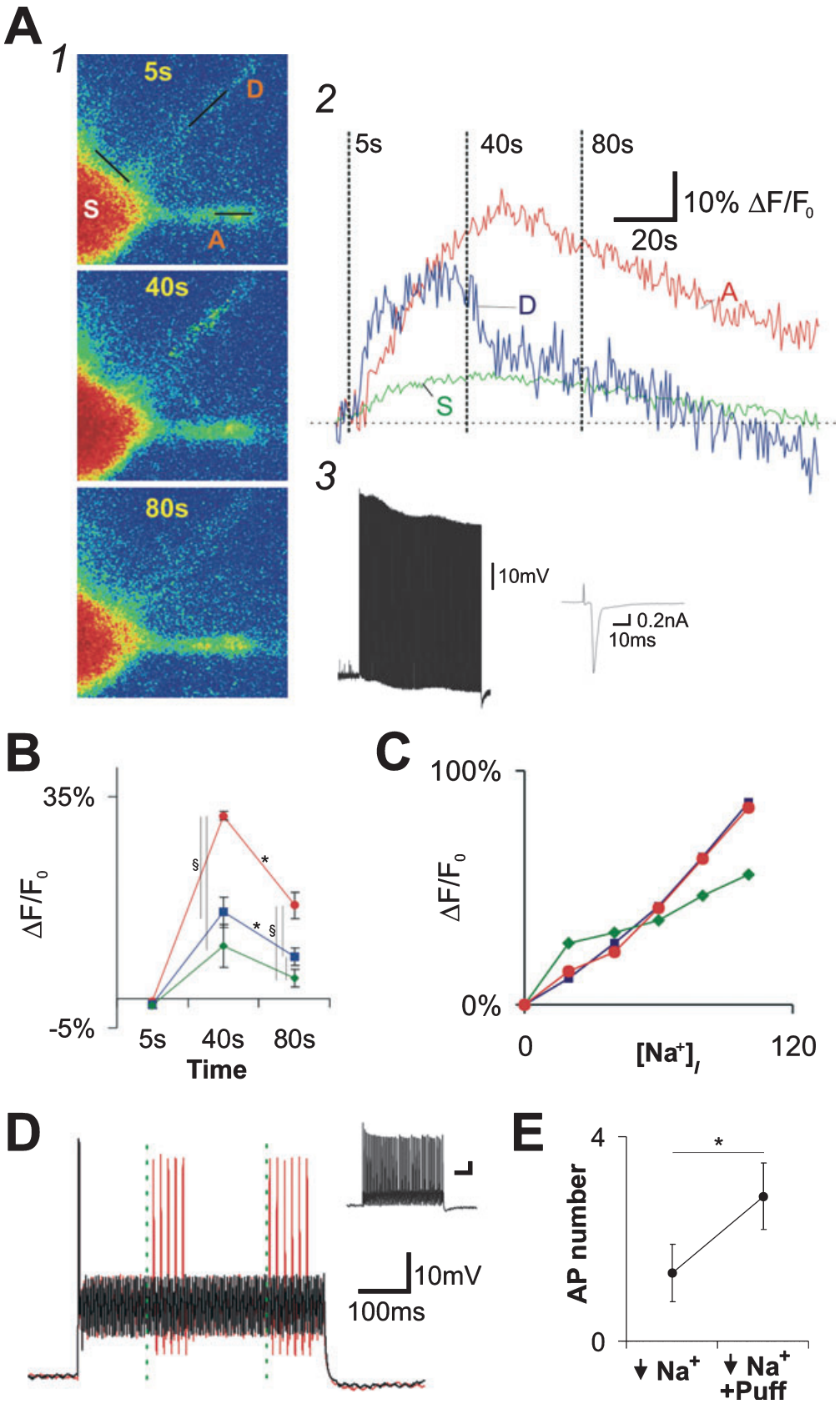

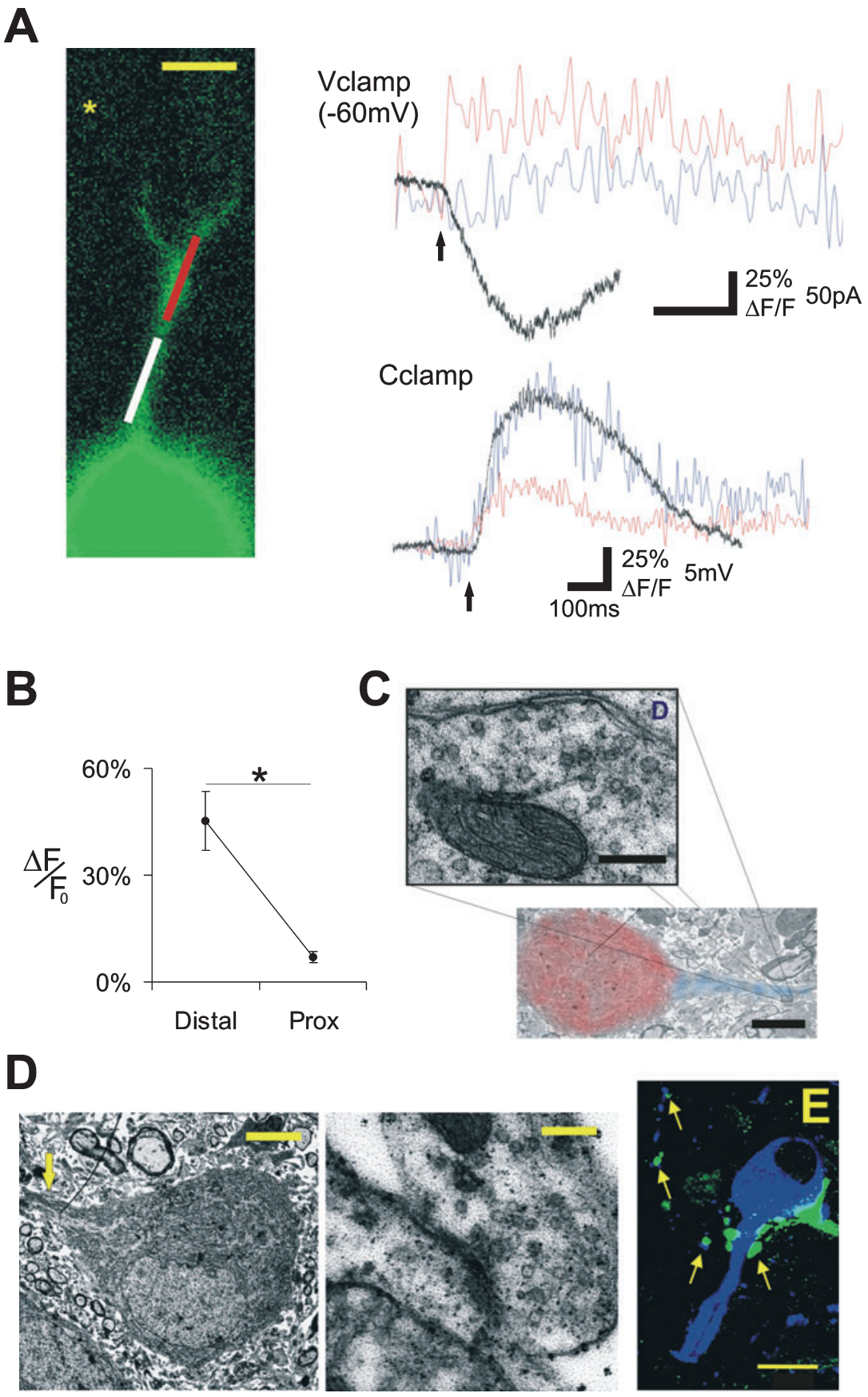

A mathematical model of MNTB neurons shows that dendritic Na^+ channels improve AP firing

In order to assess the ability of the MNTB cell model to reproduce experimental observations we applied a series of calyceal-like excitatory postsynaptic potentials (EPSPs) based on the calyx of Held synaptic model constructed by Graham *et al.* (2001). The calyx model is available for download at http://senselab.med.yale.edu/senselab/modeldb/. A two-compartment MNTB cell model (soma and axon only, axonal Na^+ conductance equal to 0.398 mS/cm^2)

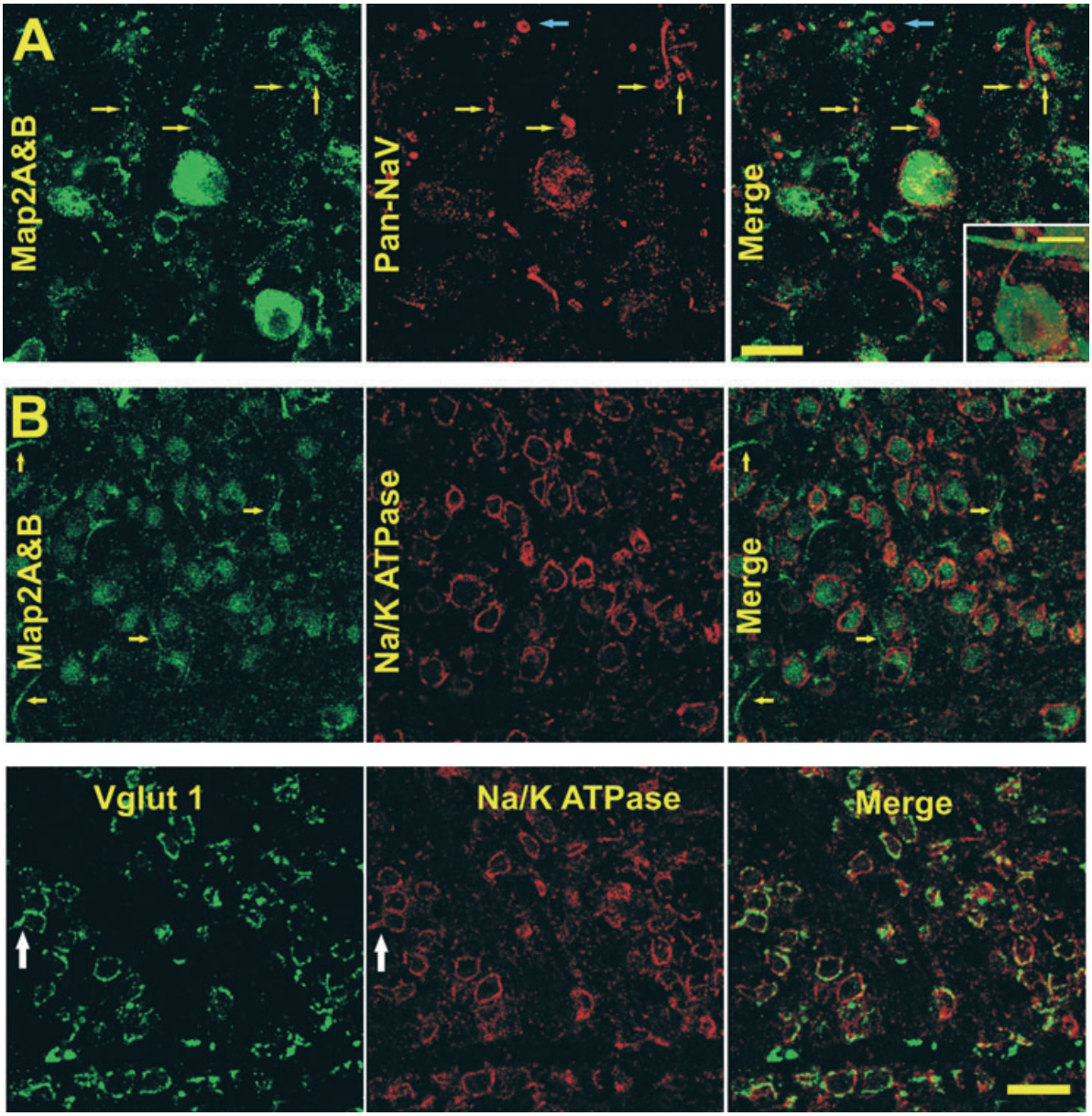

FIG. 5. NaV channels are located on dendrites and Na^+/K^+ ATPase proteins are located at the postsynaptic soma. (A) Pan-NaV labelling of MNTB cells showing the association of Na^+ channels with microtubule-associated protein (MAP)2A and B (yellow arrows) and Pan-NaV labelling with no corresponding MAP2A and B staining (blue arrow; scale bar: 20 μm). Inset: MNTB cell (*z* stack) soma and dendrite intensely labelled by anti-Pan-NaV antibodies (scale bar: 10 μm). (B) Examples of Na^+/K^+ ATPase immunoreactivity associated with the somatodendritic marker MAP2A and B (top panels) and the presynaptic terminal marker vesicular glutamate transporter (V-Glut) 1 (bottom panels). Na^+/K^+ ATPase appear to form mostly ring structures (examples dendrites marked by MAP2A and B, yellow arrows, but not labelled by anti-Na^+/K^+ ATPase antibodies). Also, tubular structures marked by the anti-Na^+/K^+ ATPase antibody were generally also marked by the V-Glut 1 antibody (white arrows).

FIG. 4. MNTB dendrites exhibit glutamate receptors. (A) Ca^{2+} indicator response to pressure-ejection of 1 mM glutamate (ejection site indicated by *, left) distally at the dendrite (line scan region, red, shown left) and proximally (scan line region shown by the white line, left). On right, top panel shows distal (red trace) and proximal (blue trace) dendritic fluorescence emission with simultaneous voltage-clamp recordings (black trace). Right bottom, same cell response on current-clamp (voltage trace shown in black). (B) Summary of $\Delta F/F_0$ on distal and proximal dendritic region (* indicates $P < 0.03$, paired *t*-test). (C) Electron microscopy photograph showing an MNTB cell soma (highlighted in red) and a dendrite (blue) and an associated synaptic button containing round vesicles (detailed at the top panel, scale bar: 0.25μm). (D) Another example of an electron micrograph of MNTB cell soma and the proximal dendrites. On left, low magnification (scale bar = 5 μm), yellow arrows indicate the sites of the synaptic contact. Right panel shows a high magnification of the button indicated on the left panel (scale bar: 0.25 μm). (E) MAP2A and B and V-Glut 1 labelling of an MNTB neuron, suggesting the presence of glutamatergic terminals associated to principal cell dendrites (scale bar: 20 μm).

reproduced all the basic firing features of normal principal cells: single APs independent of the duration of the current step and a single AP in response to one EPSP and little AP accommodation during a train of EPSPs (Fig. 6A–C). However, the addition of a passive dendrite (no dendritic NaVch) to the model impaired the cell's response to EPSPs and increased the firing threshold (the amplitude of the current step necessary for the production of one AP) from −100 pA to −150 pA, and the AP amplitude in response to current steps (from 85.5 mV to 63.8 mV, 200 pA current; Fig. 6A–C). AP accommodation was greater after the implementation of a passive dendrite in the MNTB model (1.39 without the dendrite and 1.86 with the dendrite; Fig. 6B). Addition of dendritic NaVch (10% of the axonal Na^+ channel density maintaining the total Na^+ conductance; dendritic conductance equal to 0.02 ms/cm^2 and axonal conductance equal to 0.2 ms/cm^2) restored the initial AP amplitude (83 mV) threshold (110 pA) and accommodation to levels similar to the model with no dendrite (equal to 1.2287; Fig. 6B and C). We also simulated changes in internal Na^+ concentration (see Fig. 3A; 't = 80 s') after prolonged firing. An additional 19 mM of intracellular Na^+ to the resting 9 mM Na^+ ($[Na]_{I0}$) from the K^+-gluconate of intracellular Na^+ yielded a reversal potential for Na^+ equal to 43 mV in the axon (72.9 mV in control conditions, using K^+-gluconate internal solution). Our simulation demonstrated that if the dendritic $[Na^+]_I$ is smaller than the axonal counterpart (dendritic $[Na^+]_I$ = 8.4 mM + $[Na]_{I0}$), AP amplitudes do not accommodate to the extent that a situation in which axonal and dendritic $[Na^+]_I$ are high (dendritic and axonal $[Na^+]_I$ equal to 19 mM + $[Na]_{I0}$; accommodation equal to 1.44 vs. 1.78, respectively; Fig. 6D). An active MNTB dendrite also decreased the AP time difference between the three compartments (dendrite, soma and axon) in response to somatic depolarization. In a model with a passive dendrite, the AP peak time difference between the axon and the dendrite in response to a 5-ms/200-pA current injection is equal to 0.35 ms, while this difference is equal to 0.075 ms when the dendrite was active (10% of NaVch on the dendrite; supplementary Fig. S1, D). The AP amplitude difference between dendrite and axon was also smaller on the active

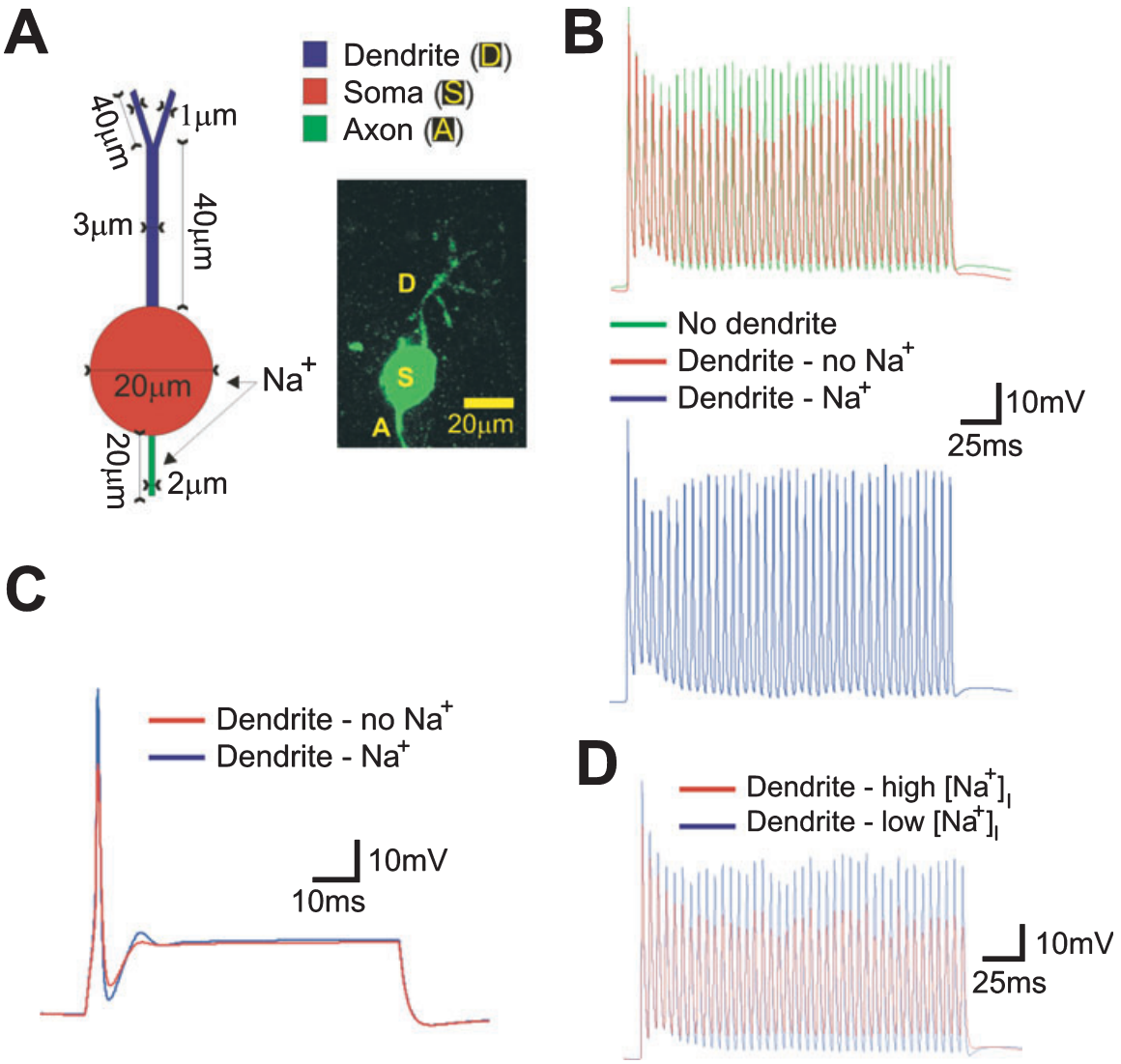

FIG. 6. MNTB compartmental models reproduce the effect of an active Na^+ conductance on the dendrite. (A) Schematic representation of our compartmental model showing lengths and diameters of different compartments (inset: a reconstructed MNTB cell with similar architecture). (B) Model response to simulated calyceal EPSPs (250 Hz), top panel shows the response of a modelled cell with no dendrite (green trace) and with a passive dendrite (red); bottom panel shows the model response when a voltage-gated Na^+ conductance was added to the dendrite (active dendrite). (C) Model response to a 300-pA current step (blue trace, active dendrite; red trace, passive dendrite). (D) MNTB cell with an active dendrite model response to 250-Hz EPSPs (simulated calyx of Held) when the internal Na^+ concentration of dendrite and axon were the same (red trace, high $[Na^+]_I$) and when the dendritic $[Na^+]_I$ was lower than the axonal concentration (blue trace).

dendrite model (22.3 mV, passive dendrite; 0.75 mV, active dendrite; supplementary Fig. S1, D). When Na gradients (ratio of internal and external [Na^+]) were different between the axon and dendrite (Na^+ reversal potential equal to 30 mV in the axon and 50 mV in the dendrite), the AP in response to a 5-ms/250-pA current injection occurred earlier than when the axon and dendrite had the same Na^+ reversal potential (supplementary Fig. S1, D).

Small densities of Na^+ channels placed on dendrites produced significant changes in AP amplitude during 200-Hz EPSPs. Supplementary Fig. S2, A shows average AP amplitudes during a 200-ms/200-Hz train of EPSPs with different NaVch densities in the dendrite. When no Na^+ channels were present at the dendrite, the mean absolute APs amplitude was bellow zero (−0.62 mV), while the mean amplitude was equal to 4.8 mV when 10% of the total number of Na^+ channels were placed on the dendritic membrane. Different NaVch kinetics models produced very similar results (we used Hodgkin and Huxley voltage-dependent Na^+ current equations included in the program Neuron and also the equations for Na^+ current described in Rothman *et al.*, 1993).

Na^+ channels in dendrites delay dendritic but not somatic EPSPs

We simulated the influence of a dendritic Na^+ current on the cell's response to EPSPs originating on the dendrites (EPSP modelled by an alpha function with time constant equal to 0.1 ms and 10 mV reversal potential). Figure 7A shows the model response to a dendritic EPSP when the dendrite was active and passive. Another possible configuration of MNTB excitatory inputs is a calyceal terminal sending small contacts to the postsynaptic dendrite (Rowland *et al.*, 2000). We tested the influence of dendritic NaVch in this pre- and postsynaptic configuration by placing 5% of the 500 active zones (Graham *et al.*, 2001) on the proximal dendrite and compared it with the MNTB model that had all active zones placed at the soma and no dendrite. The latter model implementation produced an absolute mean spike amplitude of −8.26 mV (in relation to a resting potential of −65 mV), while the former implementation yielded a mean amplitude of −1.82 mV and an AP accommodation of 1.26 (Fig. 7B).

We also implemented an MNTB cell model that includes a myelinated axon and nodes of Ranvier based on the model of axonal conductance velocity of Brill *et al.* (1977) (supplementary Fig. S2, B). Myelinated compartment(s) had lengths of 300 μm or 450 μm, the same diameter as the unmyelinated axon (1 μm), and a total leak conductance of 5.6 nS and a capacitance of 1.87 nF. Nodes of Ranvier were 4 μm long and had also 1 μm diameter, Hodgkin and Huxley Na^+ and K^+ (0.09 S/cm^2) conductances and a leak conductance of 0.09 S/cm^2. There are no morphological data on the length of the myelin or nodes of Ranvier of MNTB cells; however, MNTB axons that terminate on the ipsilateral lateral superior olive are short (about 0.5 mm in rats; Banks & Smith, 1992),, hence we implemented a model with two 300-μm myelinated compartments and two nodes or one 450-μm myelinated compartment and one node of Ranvier. A subthreshold depolarization originated at the soma, provoked a peak depolarization of 78% of the soma depolarization peak at the axon initial segment and 21.8% at the node of Ranvier in the single myelinated compartment model. The model with two myelinated compartments and two nodes produced depolarizations of 99% at the axon initial segment, 34% at the first node and 14.6% at the second node. We then compared AP amplitude at the node of Ranvier (single node model) when dendritic and axonal compartments had different or similar $[Na^+]_I$. When the dendritic Na reversal potential was equal to 50 mV and the axonal Na^+ reversal potential was equal to 30 mV, the AP amplitude at the node (in response to 400-pA current injection at the soma) was equal to −10.83 mV (resting potential equal to −65 mV) and the time to peak was equal to 2.97 ms, while when both axonal and dendritic Na^+ reversal potential were equal to 30 mV, AP amplitude and peak time were equal to −17.9 mV and 3.2 ms, respectively (supplementary Fig. S2, C). Larger spikes at the initial segment of the axon also required less NaVch at the nodes to produce large nodal APs. Using the model in which 5% of the active zones of the calyx were placed on the proximal dendrite (active dendrite model) and nodal Na^+ conductance was equal to 1.4 S/cm^2, APs were significantly larger at the node of Ranvier than when the MNTB model had no dendrite (6 mV difference on average; supplementary Fig. S2, D). Only after the nodal Na^+ conductance was set to 1.8 S/cm^2, nodal AP amplitudes of the MNTB model with and without the dendrite were similar (supplementary Fig. S2, D). We also observed a small improvement in AP jitter in response to calyceal EPSPs. During a 250-Hz (1-s) train of calyceal EPSPs, the mean nodal inter-AP time was equal to 4 ms (SD = 0.27 ms) for the calyceal/dendritic ramification model and 4.02 ms (SD = 0.29 ms) for the no dendrite model. APs elicited at the node of Ranvier (injecting depolarizing current pulses at the node) were not able to invade the soma in the model with the passive and active dendrite (supplementary Fig. S2, E).

Diffusion simulations show that Na^+ influx in dendrites is not affected by the calyx of Held

The maintenance of AP amplitude by dendritic NaVch could also be accomplished by NaVch channels placed at the soma. However, as MNTB cell somas are extensively covered by the calyx of Held, external Na^+ concentrations would rapidly change during/after prolonged stimulation (as the extracellular volume around the postsynaptic membrane facing the terminal is very limited and would be rapidly depleted of Na^+ after repetitive firing). To demonstrate that, we used a model of Na^+ diffusion in MNTB cells to assess the influence of the giant terminal on somatic Na^+ gradient (Fig. 7C). When Na^+ channels were only incorporated on the soma membrane, there was a progressive depletion of the $[Na^+]_E$ in the synaptic cleft as it enters the soma (note that there is only one Na^+ channel at the synaptic cleft; Fig. 7C). However, when Na^+ channels were distributed along the MNTB dendrite, $[Na^+]_E$ around dendrites is not severely affected (as demonstrated by a drop followed by an increase in $[Na]_E$ vs. time; Fig. 7C).

Discussion

In this work, we have demonstrated that MNTB principal cell dendrites, despite their relative shortness and simple architecture, contribute importantly to AP firing. We have used rats for this study, which have previously been shown to lack NaVch in the soma membrane (Leao *et al.*, 2005), in contrast to mice, which display a significant amount of somatic NaVch (Leao *et al.*, 2006b). We have firstly shown that fast transient inward currents are present on MNTB dendrites using outside-out patches and immunohistochemistry. These fast inward currents display all the characteristics of NaVch, which was confirmed pharmacologically in experiments using TTX application. Dendritic patches also displayed outward currents insensitive to 3 mM TEA. The nature of these currents is unknown, but they are likely to arise mainly from K^+ leak channels (Berntson, unpublished results). Inward currents could also be generated by Cd^{2+} -insensitive Ca^{2+} currents, however, Ca^{2+} currents in whole-cell recordings are quite small in MNTB cells (less than 400 pA in total; Leao *et al.*, 2004b) and, hence, it would not be possible to obtain such a large current in an Ca^{2+} outside-out patch.

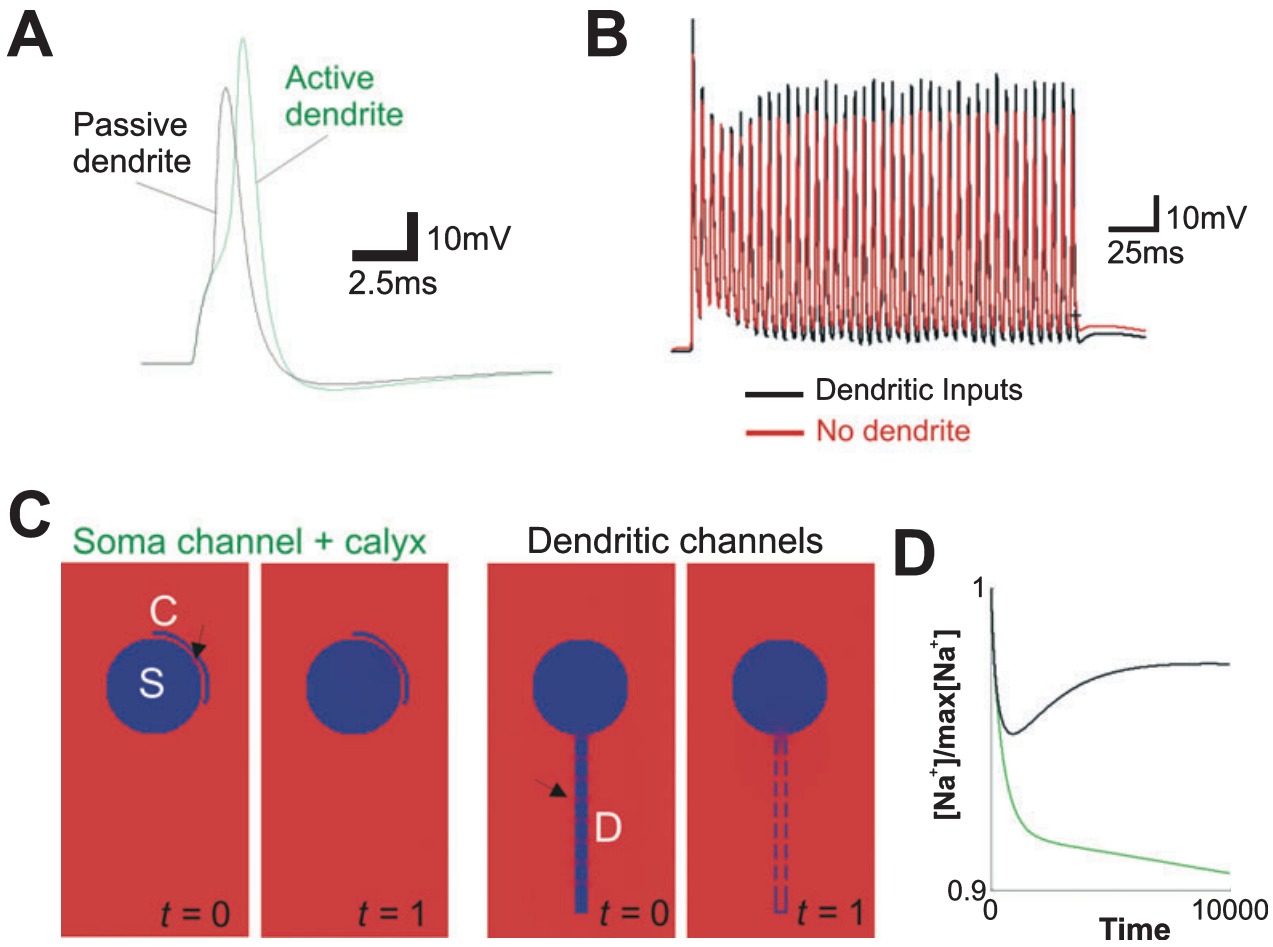

FIG. 7. Dendritic Na^+ channels maintain AP amplitude during repetitive firing. (A) Active (green trace) and passive (black trace) dendrite model response to a dendritic EPSP. (B) Model response to calyceal EPSPs when 5% of the active zones were placed on the proximal dendrite (black trace) and when the model was implemented with no dendrite (red trace). (C) Finite difference simulations of $[Na^+]$ demonstrating the restrictive effect of the calyx of Held. Figures represent cross-sections of the finite difference MNTB model showing soma (S), calyx of Held (C) and dendrite (D) (red colour represents the max $[Na^+]$ and blue colour $[Na^+]$ equal to 0). The left panels show the simulation that a Na^+ channel is placed on the postsynaptic membrane facing a 'finger' from the presynaptic terminal at $t = 0$ and $t = 1$ (arbitrary units). Right panels show the results of the simulation that Na^+ channels are placed at the dendrite ('free' of giant terminals). The arrows indicate the regions that $[Na^+]$ were measured in (C). (D) Normalized external $[Na^+]$ evolution in time (arbitrary units, measurement regions are indicated by arrows in C) for the two models (soma channel + calyx, green trace; dendritic channels, black trace).

As demonstrated by our focal TTX application experiments and modelled compartmental MNTB cell, NaVch channels in dendrites contribute to an 'attenuation' of the additional capacitance caused by the dendritic membrane, and the blocking of these channels disrupts the capacitance compensation offered by fast NaVch. We used young animals in this study, as the high level of myelination observed in older animals would make visualization of dendrites very difficult. However, as shown by outside-out patch recordings from P28 animals, the expression of NaVch in MNTB dendrites is likely to be preserved throughout adulthood.

The importance of NaVch in MNTB firing was experimentally assessed by focal application of TTX in dendrites and by the implementation of a compartmental MNTB model. Pressure application of small quantities of TTX on dendrites was unlikely to affect axonal Na^+ channels. The cells used in these experiments had the dendrites and axons running in opposite directions and, in cases that an antidromic spike was elicited, there was no effect on spike timing after TTX application (as the axonal AP threshold would be increased if NaVch in the axon were partially blocked). When TTX was ejected near the soma (and axon initial segment), MNTB cells generally hyperpolarized (see the example in Fig. 2) while dendritic application of TTX did not change the resting potential. The lack of change in resting potential was another indication that TTX was primarily affecting dendritic NaVch. Focal TTX application effects were reproduced in a compartmental MNTB model. However, elimination of NaVch in the model dendrite caused more dramatic effects in firing properties than observed after dendritic ejection of TTX (Fig. 6). This discrepancy could be explained by the fact that most of the rat MNTB cells have more than one dendrite (generally two; see histological preparations in Fig. 1A).

Dendrites across the CNS commonly express TTX-sensitive Na^+ and active dendrites have been shown to execute a variety of computational tasks in other systems (Stuart & Sakmann, 1994; Bischofberger & Jonas, 1997; Martina *et al.*, 2000) . For example, EPSPs are amplified by active dendritic conductances, increasing synaptic efficiency of distal synapses on dendrites (Oviedo & Reyes, 2002). However, the most studied aspect of dendritic function is the backpropagation of APs. Backpropagating APs have been implicated in several transmission phenomena, including dendritic neurotransmitter release (Santiago *et al.*, 1992), modulation of the cell's firing pattern (Lemon & Turner, 2000), synaptic plasticity (reviewed in Holthoff, 2004) and computation (e.g. integration, gain control) of

synaptic inputs (Mehaffey *et al.*, 2005; Ibarz *et al.*, 2006; reviewed in Gulledge *et al.*, 2005). Nevertheless, Scott *et al.* (2007) have demonstrated that, in neurons of the medial superior olive (MSO), backpropagation of APs into dendrites could impair the cell's ability to fire at high-frequency, and low-threshold voltage-gated K^+ channels are partially involved in the attenuation of backpropagating of APs (Scott *et al.*, 2007). The authors point out that backpropagating APs would affect the timing and synchrony of the neuronal input/output function (Scott *et al.*, 2007). In MNTB neurons, in contrast to MSO cells, the main source of excitation targets the soma and, due to the short dendritic length, APs at the dendrite and at the initial segment appear to occur almost simultaneously after strong calyceal depolarizations (supplementary Fig. S1, D). Thus, it is unlikely that the presence of NaVch in MNTB dendrites contributes to the generation of unsynchronized backpropagating APs. In addition, the unusually small AP amplitude in MSO somas is an impediment to the generation of strong AP in dendrites (Scott *et al.*, 2007), while somatic APs at the MNTB somas are relatively large, especially in response to calyceal depolarization (Forsythe, 1994).

In MNTB cells, NaVch in dendrites could serve as an additional source of inward currents for the maintenance of AP amplitude, especially during (and after) repetitive firing (when axonal $[Na^+]_I$ is augmented), avoiding AP failures and maintaining a low firing threshold. Larger AP amplitudes improve the propagation of information (Bollmann & Sakmann, 2005). Also, our model indicated that active MNTB dendrites could amplify APs in response to (non-calyceal) dendritic excitatory postsynaptic currents (EPSCs), while delaying AP firing, however, it would be difficult to isolate dendritic postsynaptic glutamate from somatic receptors as synaptic contacts were observed in the proximal dendrite, making the chemical isolation (e.g. by pressure-ejecting CNQX) impossible. Hamann *et al.* (2003) demonstrated in a previous study that non-calyceal EPSPs generate postsynaptic APs with longer latencies than calyceal ones (Hamann *et al.*, 2003). Our compartmental MNTB model shows that an active MNTB dendrite amplifies and delays APs in response to dendritic EPSPs with no interference in AP timing during calyceal EPSPs. The additional AP delay in response to dendritic EPSPs would allow the auditory system to distinguish between a calyceal (nearly instantaneous) and a non-calyceal input (delayed). This dual response modality is additional evidence that MNTB function is more than to simply relay (and invert) information from the anteroventral cochlear nucleus (Kopp-Scheinpflug *et al.*, 2003). Also, there is some anatomical evidence that the calyx of Held makes contact with proximal postsynaptic dendrites (Morest, 1968; Rowland *et al.*, 2000; von Gersdorff & Borst, 2002). In this is the case, dendritic Na^+ channels would help to maintain AP amplitude during repetitive firing in response to calyceal EPSCs. It seems metabolically advantageous to increase the AP amplitude at the axonal initial segment, as fewer NaVchs at the node of Ranvier are necessary to transmit large depolarizations (supplementary Fig. S2, D) that, in turn, increase release probability at the synaptic terminal.

Postsynaptic mechanisms that contribute to the maintenance of AP amplitude are essential features in cells that need to transmit information with precise timing (Bollmann & Sakmann, 2005). Larger depolarizations at the presynaptic terminal increase the probability of release of neurotransmitters (Bollmann & Sakmann, 2005). In addition, successful propagation of APs across myelinated (and unmyelinated) fibres depends directly on the initial amplitude of the AP (Khaliq & Raman, 2005). Initially, large calyceal EPSCs (several nA) would force the generation of large APs. However, calyceal EPSPs undergo rapid depression during repetitive firing (Forsythe, 1994; von Gersdorff & Borst, 2002; Hermann *et al.*, 2007). It has been shown recently that, *in vivo*, MNTB cells fire at an average of 25 Hz (Hermann *et al.*, 2007). Hence, during normal activity, calyceal EPSCs would not reach the large amplitudes observed in acute slices and the maintenance of AP amplitudes in response to depressed calyceal EPSCs would greatly contribute to high-fidelity transmission.

Our Na^+ imaging results indicate that clearance of intracellular Na^+ is faster in dendrites and soma than in axons. Clearance differences are likely to be related to the exclusively somatic localization of Na^+/K^+ ATPase (also demonstrated in a previous work; Kim *et al.*, 2007), associated with a larger dendritic diameter (compared with the axon) and a possible, lower concentration of NaVch on dendrites. Na^+/K^+ ATPase localized at the soma may contribute to the regulation of $[Na^+]$ and $[K^+]$ at the 'vast' calyceal cleft, preventing the accumulation of K^+ and exhaustion of Na^+ at the extracellular space covered by the calyceal synapse. Changes in ionic concentrations (and their consequences) at synaptic clefts have been known for decades (Matiushkin, 1976). In a synapse as large as the calyx of Held, maintenance of ionic gradients is crucial for high-fidelity transmission. Hence, 'back-up' NaVch in dendrites rather than somas would allow a better 'access' to extracellular Na^+ without the constraining presence of the calyx and would minimize the changes in Na^+ concentrations at the cleft, that could also affect the presynaptic terminal excitability. The calyx of Held fenestration observed during MNTB development may contribute to ionic clearance; nevertheless, the area of the 'finger-like' calyx of Held facing the postsynaptic cell is still many orders of magnitude greater than usual synapses (von von Gersdorff & Borst, 2002). In contrast to the results shown here, we have previously detected the presence of small Na^+ currents in somatic membranes of mice MNTB cells (Leao *et al.*, 2006b). These currents, however, were quite small when compared with Na^+ currents recorded from dendritic membranes and may not produce a significant ionic imbalance around the calyceal cleft (Leao *et al.*, 2006b). Additionally, the currents recorded in our previous work in mice could also have been partially produced by axonal or dendritic channels that could have been excised together to somatic channels during outside-out patch recordings or cell dissociation (Leao *et al.*, 2006b).

MNTB neurons exhibit a variety of specializations dedicated to faithfully transmit information (e.g. Kv1 and Kv3.1 channels, resurgent and persistent Na^+ currents; Dodson *et al.*, 2002; Leao *et al.*, 2006b), and an active MNTB dendrite may contribute to the postsynaptic machinery that permits reliable postsynaptic firing. Our results provide an example of a simple dendrite capable of performing complex computational tasks.

Supplementary material

The following supplementary material may be found on http://www.blackwell-synergy.com

Fig. S1. Na^+ channels are present on dendritic MNTB of P28 rats.

Fig. S2. Active MNTB improves action potential (AP) timing and propagation.

Please note: Blackwell Publishing are not responsible for the content or functionality of any supplementary materials supplied by the authors. Any queries (other than missing material) should be directed to the correspondence author for the article.

Acknowledgements

We would like to thank Dr Cathy Gillespie of the Electron Microscopy Unit of the John Curtin School of Medical Research for performing the electron microscopy in this study, and Dr Henrique Von Gersdorff for the helpful comments on the manuscript.

Grants

Luciano da F. Costa was financially supported by CNPq (308231/03-1) and FAPESP (05/00587-5).

Abbreviations

ACSF, artificial cerebrospinal fluid; AP, action potential; EPSC, excitatory postsynaptic current; EPSP, excitatory postsynaptic potential; MAP, microtubule-associated protein; MNTB, medial nucleus of the trapezoid body; MSO, medial superior olive; NaVch, voltage-gated Na^+ channels; PBS, phosphate-buffered saline; TEA, tetraethyl ammonium; TTX, tetrodotoxin; V-Glut, vesicular glutamate transporter.

References

Banks, M.I. & Smith, P.H. (1992) Intracellular recordings from neurobiotin-labelled cells in brain slices of the rat medial nucleus of the trapezoid body. *J. Neurosci.*, **12**, 2819–2837.

Bischofberger, J. & Jonas, P. (1997) Action potential propagation into the presynaptic dendrites of rat mitral cells. *J. Physiol.*, **504**, 359–365.

Bollmann, J.H. & Sakmann, B. (2005) Control of synaptic strength and timing by the release-site Ca^{2+} signal. *Nat. Neurosci.*, **8**, 426–434.

Brill, M.H., Waxman, S.G., Moore, J.W. & Joyner, R.W. (1977) Conduction velocity and spike configuration in myelinated fibres: computed dependence on internode distance. *J. Neurol. Neurosurg. Psychiatry*, **40**, 769–774.

Dodson, P.D., Barker, M.C. & Forsythe, I.D. (2002) Two heteromeric Kv1 potassium channels differentially regulate action potential firing. *J. Neurosci.*, **22**, 6953–6961.

Dugandzija-Novaković, S., Koszowski, A.G., Levinson, S.R. & Shrager, P. (1995) Clustering of Na^+ channels and node of Ranvier formation in remyelinating axons. *J. Neurosci.*, **15**, 492–503.

Forsythe, I.D. (1994) Direct patch recording from identified presynaptic terminals mediating glutamatergic EPSCs in the rat CNS, in vitro. *J. Physiol.*, **479**, 381–387.

von Gersdorff, H. & Borst, J.G. (2002) Short-term plasticity at the calyx of Held. *Nat. Rev. Neurosci.*, **3**, 53–64.

Goodman, J.A., Kroenke, C.D., Brethorst, G.L., Ackerman, J.J. & Neil, J.J. (2005) Sodium ion apparent diffusion coefficient in living rat brain. *Magn. Reson. Med.*, **53**, 1040–1045.

Graham, B.P., Wong, A.Y.C. & Forsythe, I.D. (2001) A computational model of synaptic transmission at the calyx of Held. *Neurocomputing*, **38**, 37–42.

Gulledge, A.T., Kampa, B.M. & Stuart, G.J. (2005) Synaptic integration in dendritic trees. *J. Neurobiol.*, **64**, 75–90.

Hamann, M., Billups, B. & Forsythe, I.D. (2003) Non-calyceal excitatory inputs mediate low fidelity synaptic transmission in rat auditory brainstem slices. *Eur. J. Neurosci.*, **18**, 2899–2902.

Hermann, J., Pecka, M., von Gersdorff, H., Grothe, B. & Klug, A. (2007) Synaptic transmission at the calyx of Held under in vivo like activity levels. *J. Neurophysiol.*, **98**, 807–820.

Hieber, V., Siegel, G.J., Fink, D.J., Beaty, M.W. & Mata, M. (1991) Differential distribution of (Na, K)-ATPase alpha isoforms in the central nervous system. *Cell. Mol. Neurobiol.*, **11**, 253–262.

Hines, M.L. & Carnevale, N.T. (2001) NEURON: a tool for neuroscientists. *Neuroscientist*, **7**, 123–135.

Holthoff, K. (2004) Regenerative dendritic spikes and synaptic plasticity. *Curr. Neurovasc. Res.*, **1**, 381–387.

Ibarz, J.M., Makarova, I. & Herreras, O. (2006) Relation of apical dendritic spikes to output decision in CA1 pyramidal cells during synchronous activation: a computational study. *Eur. J. Neurosci.*, **23**, 1219–1233.

Khaliq, Z.M. & Raman, I.M. (2005) Axonal propagation of simple and complex spikes in cerebellar Purkinje neurons. *J. Neurosci.*, **25**, 454–463.

Kim, J.H., Sizov, I., Dobretsov, M. & von Gersdorff, H. (2007) Presynaptic Ca^{2+} buffers control the strength of a fast post-tetanic hyperpolarization mediated by the alpha3 Na(+)/K(+)-ATPase. *Nat. Neurosci.*, **10**, 196–205.

Kopp-Scheinpflug, C., Lippe, W.R., Dorrscheidt, G.J. & Rubsamen, R. (2003) The medial nucleus of the trapezoid body in the gerbil is more than a relay: comparison of pre- and postsynaptic activity. *J. Assoc. Res. Otolaryngol.*, **4**, 1–23.

Leao, R.N., Oleskevich, S., Sun, H., Bautista, M., Fyffe, R.E. & Walmsley, B. (2004a) Differences in glycinergic mIPSCs in the auditory brain stem of normal and congenitally deaf neonatal mice. *J. Neurophysiol.*, **91**, 1006–1012.

Leao, R.N., Berntson, A., Forsythe, I.D. & Walmsley, B. (2004b) Reduced low-voltage activated K+ conductances and enhanced central excitability in a congenitally deaf (dn/dn) mouse. *J. Physiol.*, **559**, 25–33.

Leao, R.M., Kushmerick, C., Pinaud, R., Renden, R., Li, G.L., Taschenberger, H., Spirou, G., Levinson, S.R. & von Gersdorff, H. (2005) Presynaptic Na^+ channels: locus, development, and recovery from inactivation at a high-fidelity synapse. *J. Neurosci.*, **25**, 3724–3738.

Leao, R.N., Sun, H., Svahn, K., Berntson, A., Youssoufian, M., Paolini, A.G., Fyffe, R.E. & Walmsley, B. (2006a) Topographic organization in the auditory brainstem of juvenile mice is disrupted in congenital deafness. *J. Physiol.*, **571**, 563–578.

Leao, R.N., Naves, M.M., Leao, K.E. & Walmsley, B. (2006b) Altered sodium currents in auditory neurons of congenitally deaf mice. *Eur. J. Neurosci.*, **24**, 1137–1146.

Lemon, N. & Turner, R.W. (2000) Conditional spike backpropagation generates burst discharge in a sensory neuron. *J. Neurophysiol.*, **84**, 1519–1530.

Martina, M., Vida, I. & Jonas, P. (2000) Distal initiation and active propagation of action potentials in interneuron dendrites. *Science*, **287**, 295–300.

Matiushkin, D.P. (1976) Reactions of nervous elements to K+ accumulation in the medium and functional potassium feedback at the synapse. *Fiziol. Zh. SSSR Im. I. M. Sechenova*, **62**, 1834–1841.

Mehaffey, W.H., Doiron, B., Maler, L. & Turner, R.W. (2005) Deterministic multiplicative gain control with active dendrites. *J. Neurosci.*, **25**, 9968–9977.

Meier, S.D., Kovalchuk, Y. & Rose, C.R. (2006) Properties of the new fluorescent Na^+ indicator CoroNa Green: Comparison with SBFI and confocal Na^+ imaging. *J. Neurosci. Methods*, **155**, 251–259.

Morest, D.K. (1968) The growth of synaptic endings in the mammalian brain: a study of the calyces of the trapezoid body. *Z Anat. Entwicklungsgesch.*, **127**, 201–220.

Oviedo, H. & Reyes, A.D. (2002) Boosting of neuronal firing evoked with asynchronous and synchronous inputs to the dendrite. *Nat. Neurosci.*, **5**, 261–266.

Raman, I.M. & Bean, B.P. (2001) Inactivation and recovery of sodium currents in cerebellar Purkinje neurons: evidence for two mechanisms. *Biophys. J.*, **80**, 729–737.

Rothman, J.S., Young, E.D. & Manis, P.B. (1993) Convergence of auditory nerve fibers onto bushy cells in the ventral cochlear nucleus: implications of a computational model. *J. Neurophysiol.*, **70**, 2562–2583.

Rowland, K.C., Irby, N.K. & Spirou, G.A. (2000) Specialized synapse-associated structures within the calyx of Held. *J. Neurosci.*, **20**, 9135–9144.

Santiago, M., Machado, A. & Cano, J. (1992) Fast sodium channel dependency of the somatodendritic release of dopamine in the rat's brain. *Neurosci. Lett.*, **148**, 145–147.

Satzler, K., Sohl, L.F., Bollmann, J.H, Borst, J.G., Frotscher, M., Sakmann, B. & Lubke, J.H. (2002) Three-dimensional reconstruction of a calyx of Held and its postsynaptic principal neuron in the medial nucleus of the trapezoid body. *J. Neurosci.*, **22**, 10567–10579.

Scott, L.L., Hage, T.A. & Golding, N.L. (2007) Weak action potential backpropagation is associated with high-frequency axonal firing capability in principal neurons of the gerbil medical superior olive. *J. Physiol.*, **583**, 647–661.

Shu, Y., Duque, A., Yu, Y., Haider, B. & McCormick, D.A. (2007) Properties of action-potential initiation in neocortical pyramidal cells: evidence from whole cell axon recordings. *J. Neurophysiol.*, **97**, 746–760.

Smith, P.H., Joris, P.X. & Yin, T.C. (1998) Anatomy and physiology of principal cells of the medial nucleus of the trapezoid body (MNTB) of the cat. *J. Neurophysiol.*, **79**, 3127–3142.

Stuart, G.J. & Sakmann, B. (1994) Active propagation of somatic action potentials into neocortical pyramidal cell dendrites. *Nature*, **367**, 69–72.

Vater, M. (1995) Ultrastructural and immunocytochemical observations on the superior olivary complex of the mustached bat. *J. Comp. Neurol.*, **358**, 155–180.

Wang, L.Y., Gan, L., Forsythe, I.D. & Kaczmarek, L.K. (1998) Contribution of the Kv3.1 potassium channel to high-frequency firing in mouse auditory neurones. *J. Physiol.*, **509**, 183–194.

Youssoufian, M., Oleskevich, S. & Walmsley, B. (2005) Development of a robust central auditory synapse in congenital deafness. *J. Neurophysiol.*, **94**, 3168–3180.